Nanoscale

Accepted Manuscript

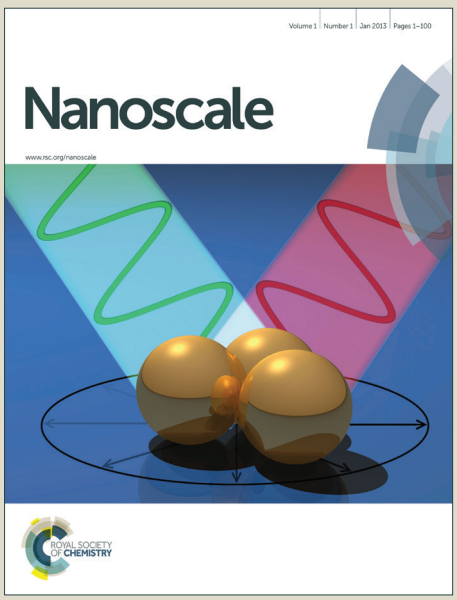

ROYAL SOCIETY OF CHEMISTRY

www.rsc.org/nanoscale

Journal Name

ARTICLE

Structural Defects Induced Peak Splitting in Gold-Copper Bimetallic Nanorods during Growth by Single Particle Spectroscopy

Received 00th January 20xx,
Accepted 00th January 20xx

DOI: 10.1039/x0xx00000x

www.rsc.org/

Sravan Thota[a‡], Shutang Chen[a‡], Yadong Zhou[b], Yong Zhang[c], Shengli Zou[b], and Jing Zhao[a,d*]

Single particle level study of the bimetallic nanoparticle growth provides valuable information that is usually hidden in ensemble measurements, helping to improve the understanding of reaction mechanism and overcome the synthetic challenges. In this study, we use single particle spectroscopy to monitor the changes in the scattering spectra of Au-Cu alloy nanorods during growth. We found that the unique features of the single particle scattering spectra were due to atomic level geometric defects in the nanorods. Electrodynamics simulations have demonstrated that small structural defects of a few atomic layers split the scattering peaks, giving rise to higher order modes, which do not exist in defect-free rods of similar geometry. The study shows that single particle scattering technique is as sensitive as high-resolution electron microscopy in revealing atomic level structural defects.

Introduction

Bimetallic nanoparticles (NPs) often exhibit highly tunable electric, magnetic, optical and catalytic properties due to the synergetic interaction between the two metals[1-6], which are very different from those of the individual components. These unique features make them promising materials in many fields including electronics, biological, and energy applications[7-11]. Currently, many efforts have been made to synthesize bimetallic NPs with controlled distribution and morphology of individual components, in order to obtain desired properties[12, 13]. However, combining two components in one structure still present synthetic challenges, because it is difficult to synchronously control the nucleation and growth of two different metals due to their distinct kinetic and thermodynamic characteristics under the same reaction conditions[14]. Moreover, different lattice parameters of the two metals pose inherent difficulties in the synthesis and lead to structural defects in bimetallic NPs[15, 16].

Over the past two decades, a variety of bimetallic structures have been generated such as core@shell[17, 18], heterostructure[13, 19], and alloyed NPs[20]. In bimetallic alloy NPs, structural instabilities/defects are commonly observed during the alloy process[21]. The defects likely arise from lattice strain created by the mismatch of lattice parameters when combining the two metals. For example, in Au-Pd[22] and Au-Cu[23] alloy NPs, lattice strain builds up due to different atomic radii, leading to defects in the structure. Even in systems like Au-Ag[24] alloy NPs, where the lattice constants are similar, vacancy sites at bimetallic interface before alloying evolve to the surface in alloying process, resulting in defects formation because of the difference in the lattice energy of the two metals. Detailed studies of these structural defects at the atomic level will help to overcome the synthetic challenges.

To reveal the structural defects, single particle methods are preferred, due to the inevitable structural heterogeneity in NP synthesis[25, 26]. Structures of single NPs are often directly measured by high-resolution transmission electron microscopy (HRTEM)[27-29]. An alternative, indirect single particle approach is dark field scattering. The scattering of metal NPs resulted from the collective oscillation of electrons induced by electromagnetic field, known as LSPR (localized surface plasmon resonance). Because the scattering of single metallic NPs is extremely sensitive to their geometry and composition[30-32], dark field scattering is suitable to monitor small structural changes during NP synthesis. For examples, atomic level changes in Au nanorods[33] or Ag nanospheres[34] during reactions have been detected with dark field scattering. Recently reported new approach, scanning probe block copolymer lithography (SPBCL),[35, 36] allows for synthesizing single multimetallic NPs at specific sites. It provides an excellent opportunity to study the detailed in-situ single particle growth process when combined with dark filed scattering technique.

[a] *Department of Chemistry, University of Connecticut*
55 North Eagleville Road, Storrs, CT 06269 (USA)
E-mail: jing.zhao@uconn.edu
[d] *Institute of Material Science, University Of Connecticut*
Storrs, CT 06269 (USA)
[b] *Department of Chemistry, University of Central Florida*
4104 Libra Drive, Orlando, Florida- 32816- 2366 (USA)
[c] *Centre for Material Science and Engineering*
Massachusetts Institute of Technology
77 Massachusetts Avenue, Cambridge, Massachusetts 02139(USA)
† Electronic Supporting information for this article is available via a link at the end of the document.
‡ These authors contributed equally to this work.

In this work, we apply the simple and non-destructive dark-field scattering spectroscopy technique and electrodynamics simulations to investigate the structure and composition change of single Au-Cu alloy nanorod during synthesis, in conjunction with traditional ensemble UV-Vis spectroscopy, X-ray Diffraction (XRD), and high angle annular dark field scanning transmission electron microscopy (HAADF-STEM) methods. The single particle scattering spectra of NPs acquired at varying reaction times display dramatically different spectral patterns from the corresponding ensemble UV-Vis spectra. Together with electrodynamics simulations, the single particle scattering study showed that the asymmetric elemental distribution and shape of the nanorods at earlier growth stage lead to split in the scattering peak of the nanorods. More importantly, small geometric defects in the nanorods composed of only several atomic layers dramatically varied the scattering spectral pattern of single nanorods. The atomic level defects in the nanorods revealed by the spectroscopy technique provide valuable information to the understanding of bimetallic NP growth.

Experimental Section

Chemicals

Gold (III) chloride trihydrate, copper (II) acetyl acetonate (97%), octadecylamine (90%), oleylamine (70%) were purchased from sigma Aldrich and used without any further purification. Tetradecylamine (95%) was obtained from TCI and used as received.

Synthesis of Au-Cu Bimetallic Nanorods

The gold copper bimetallic nanorods were synthesized following a method reported by Chen et al[37] with some modifications. Tetradecylamine (10 mmol, 2.1341 g), octadecylamine (10mmol, 2.6951 g) and gold (III) chloride trihydrate (0.05 mmol, 19.7 mg) were loaded into a flask under nitrogen protection at 160° C to form gold seeds. The reaction temperature was increased to 180° C and copper (II) acetyl acetonate in 1 mL olelyamine was injected. The solution mixture was maintained at 180° C and samples were collected at different times (2, 5, 10 and 20 minutes) during the growth. The collected samples were cooled to 150° C and toluene was added, followed by centrifugation for 2 minutes (3300 rpm). They were dispersed in nonpolar solvents such as toluene and hexane and used for further characterization.

Dark Field Scattering

The collected bimetallic NP solution was highly diluted in toluene and drop coated onto a precleaned No.1 cover glass (Fisher Scientific). The sample was allowed to air dry for a few minutes and was mounted onto a Nikon Ti-u microscope with halogen lamp as unpolarized illumination source for optical studies. Dark field condenser (NA 0.85) was adjusted to focus at the specimen plane. A 100X NA 0.8 objective (variable NA 0.8-1.3) was used to collect the light scattered only from the sample. The collected signal was directed onto the entrance slit of a spectrograph (Isoplane SCT 320, Princeton Instruments) equipped with a CCD camera (PIXIS 1024 BR, Princeton Instruments). The obtained scattering spectra from the single particles were corrected by subtracting and dividing the background, collected from a nearby region without any particles.

Instrumentation

UV-Vis spectrometer (Cary 60, Agilent technologies) was used to measure the extinction spectra of the NPs. A Rigaku ultima IV power X-ray Diffractometer with Cu Kα radiation operated at a tube voltage of 40 KV and current of 44mA was used to obtain XRD patterns. TEM images were captured using a Tecnai T-12 operated at 120 KV. HAADF-STEM image was obtained using JEOL 2010 microscope at an accelerating voltage of 200 KV.

Computational Methods

The discrete dipole approximation (DDA) method is used in the calculations[38]. The DDA method is a finite element method in which the target particle is divided into N polarizable cubes. The interactions between cubes are treated using dipole approximation. The method is accurate as long as the cube grid length is small enough. In the calculations, we used a grid length of 0.25 nm, which is close to the van der Waals diameter of gold and copper atoms for the convergence of the calculations. The dielectric constants of gold and copper are obtained from Palik's handbook[39]. The dielectric constants of the alloy are calculated by averaging dielectric constants of the two metals over their volumes. All the calculations are based on classical electrodynamics theory.

Results and Discussion

Structure and Composition of the Nanoparticles

To monitor the Au-Cu nanorod formation, we collected aliquots at 2, 5, 10, 20 minutes after the injection of Cu precursors. Figure 1A–1E show the STEM characterization of the products acquired. At the initial stage, 10 nm Au seeds were formed, as shown in Figure 1A. After injection of Cu precursors into the seed solution, quasi-nanorods of 18.2±1.6 nm in length are formed at 2 minutes reaction (Figure 1B) and grew into regular nanorod shape of 27.3±2.7 nm in length by 5 minutes (Figure 1C). And finally 36.5±4.1 nm long Au-Cu nanorods were obtained after 20 minutes of reaction (Figure 1E and Supporting information Figure S1). Different contrasts in STEM images clearly indicated the composition evolution process from bright spherical Au seeds to Au-Cu alloy nanorods. XRD results also demonstrated the composition transformation of the NPs via fcc Au phase to $AuCu_3$ phase (Figure 1F). In the XRD pattern of Au seeds (black line), three typical peaks were indexed as Au fcc phase (JCPDS: 04-0784). After the reaction of Au seeds with Cu precursor for 2 minutes, Au rich multiple fcc phases were formed as indicted by its broad XRD pattern (red line). For the 5-minute sample, the XRD pattern shifted towards Cu (JCPDS: 04-0836) rich multiple fcc phases (blue line). As the reaction proceeded to 10 minutes, the broad peaks in the XRD patterns of the 2- and 5-minute samples became narrow, indicating multiple phases turned into a single Cu

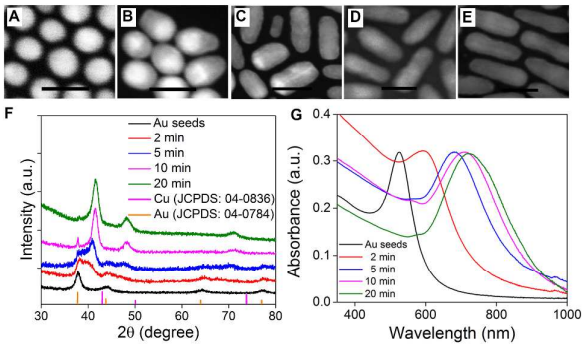

Figure 1. STEM images of samples: (A) Au seeds, and aliquots acquired at different reaction times after the injection of Cu precursors (B) 2 minutes, (C) 5 minutes, (D) 10 minutes, and (E) 20 minutes; (F) their corresponding XRD patterns and (G) UV-Vis-NIR spectra of the samples. All scale bars = 20 nm.

rich phase (pink line). After 20 minutes of reaction, pure $AuCu_3$ phase (JCPDS: 35-1357) of samples was observed, which is consistent with the STEM analysis. The corresponding UV-Vis-NIR spectra of the samples showed a red shift in the peak from 524 nm (Au seeds) to 722 nm ($AuCu_3$ nanorods), as shown in Figure 1G. The structural and composition changes in the Au-Cu nanorods growth process are consistent with previous studies[37]. However, the detailed structural change at the single particle level during the growth process cannot be easily resolved from these methods.

Single Particle Scattering Spectroscopy

Conventional optical methods measure the average signal from a large number of NPs, which only disclose macroscopic information. In order to look into the reaction at the single NP level, 100-120 NPs from each sample collected at 2, 5, 10 and 20 minutes were analyzed by dark field scattering spectroscopy. Interestingly, the single NPs displayed distinct spectral features different from the ensemble and also from each other, especially in the peak patterns. The NPs obtained from different reaction times were broadly classified into four types as shown in Figure 2 based on the scattering maximum of the major peak. Ten spectra, from each type were selected randomly from different regions on the glass substrate to represent all major spectral trends observed, as shown in Figure 2(A-D).

Nanoparticles with the major peak around 540 nm, 620 nm and 680 nm were classified as type I, II and III, respectively. All the NPs of the three spectral types were obtained from 2, 5 and 10-minute samples. The continuous red shift in the major peak clearly demonstrates the transformation of the NP shape from spherical Au seeds into Au-Cu alloy rods, after addition of the Cu precursor. Quite surprisingly, very few NPs of these types (I, II, III) have scattering spectra with a single peak (Figure 2A-C, spectra 1-2). Instead, majority population showed multiple peak patterns (Figure 2A-C, spectra 3-10). The multiple peak features are clearly resolved into three peak patterns for some NPs (4-8 of 2A-C). The peaks are around 550±7 nm, 615±13 nm and 693±16 nm with varying relative intensities. The multiple peak patterns are different from what has been found in the scattering spectra of perfect single Au nanorods, where only a single peak from the longitudinal mode of the rods was dominant[40, 41]. The NPs showing a major peak around 690-700 nm, with an additional peak to the blue of the main peak are considered type IV, as shown in Figure 2D. The number of scattering peaks of single NPs decreases as the reaction time proceeds. The reaction was completed after 20 minutes as no further changes in the spectral features was observed.

The distribution of the NPs into varying growth stages from the 2,5,10 and 20 minute-samples are listed in Table 1. As Table 1 shows, the samples acquired at the same reaction time contain NPs in two growth stages (except for the 20-minute sample). In addition, the fraction of NPs in a certain growth stage varies significantly with growth time. For example, in the 2-minute sample, 71% of the studied NPs were in growth stage I, while 29% were in growth stage II. In contrast, in the 5-minute sample, none of the observed NPs were in growth stage I; only 38% were in growth stage II and 62% were in growth stage III. The quantitative analysis of the NP distribution in varying growth stages showed that as the reaction progressed, more of the NPs were found to be in later growth stages and they all converted to the final product, eventually. The single particle measurements revealed that NPs acquired at same reaction times were not necessarily in the same growth stages, showing the variation in the reaction kinetics at the single particle level.

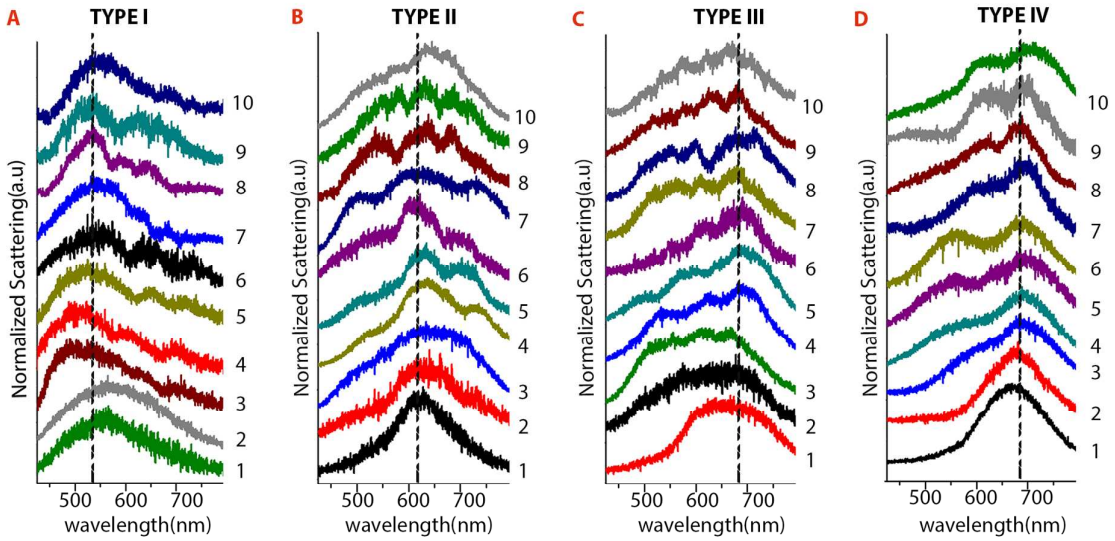

Figure 2. Single nanoparticle dark-field scattering spectra of Au-Cu alloy nanoparticles. The samples were acquired at different reaction times after injecting the copper precursors. (A) spectral type I contains nanoparticles from 2 minutes reaction, (B) spectral type II contains nanoparticles from 2 and 5 minutes reaction, (C) spectral type III contains nanoparticles from 5 and 10 minutes reaction and (D) spectral type IV contains nanoparticles from 10 and 20 minutes reaction.

Table 1. Population distribution of nanoparticles of different spectral types

	Type I	Type II	Type III	Type IV
2 minutes	71 %	29%		
5 minutes		38%	62%	
10 minutes			26%	74%
20 minutes				100%

Structural Defects Revealed by Single Particle Scattering Patterns

The spectral changes of the NPs acquired at different reaction times are associated with the structural and composition change of the NPs during the reaction. The STEM study showed that quasi-rod structure was formed at the beginning of Au-Cu nanorod growth. In order to understand the origin of the scattering peaks of these quasi-rods, discrete dipole approximation (DDA) calculations[38] were performed. From Figure 3B, the Au seed preserves its spherical shape, while Cu is deposited on one side of the Au seed. Therefore, in the theoretical modeling, we constructed a NP of similar structure with an Au sphere of 10 nm diameter being on one side, and a cone like Cu structure on the other side (as seen in Figure 3A). The calculated spectra of the transverse mode show one resonance peak at the wavelength close to that of the Au seed, ~ 520 nm. On the contrary, the longitudinal mode displays two resonance peaks as shown in Figure 3C. The dipole peak of the longitudinal mode is at ~ 593 nm and a quadrupole mode appears at ~ 530 nm (as shown in Figure S2 in supporting information). The appearance of the quadrupole mode in such a short rod is due to the asymmetric shape of the quasi rod. The field distributions in the quasi-rod (as shown in figure S2) indicate the quadrupole mode might be an anti-bonding mode of coupling between the Au and Cu NPs. Notice that the scattering efficiency of the transverse mode is much smaller than that of the longitudinal mode; the longitudinal mode dominates the scattering spectrum. When varying the size of the Cu-cone in the quasi-rod, the relative intensity of the peaks changes while the peak position is maintained (see Figure S3 in Supporting Information). The low intensity peaks at wavelengths over 600 nm shown in NPs of spectral type I may be from the longitudinal dipole peak of longer quasi-rods. In addition, if small structural defects exist in the rods (as discussed below), the dipole peak will further split, resulting in multiple weak peaks above 600 nm. Overall, the asymmetric Au-Cu rod has a main peak at ~ 540 nm and a shoulder at ~ 600 nm, consistent with the observed scattering spectra in type I.

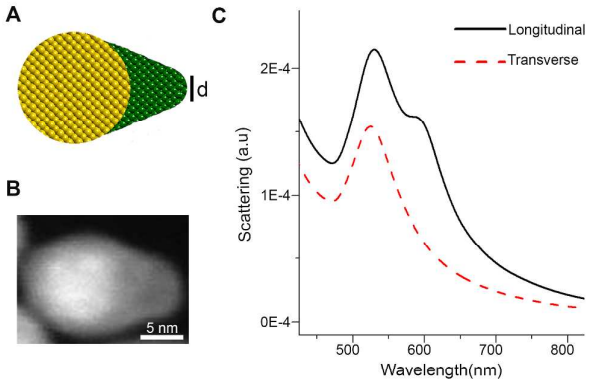

Figure 3. (A) Scheme of a quasi-rod particle. An Au sphere of 10 nm diameter is on one side (yellow) and cone-like Cu particle with d = 2 nm is on the other side (green). (B) STEM image of a quasi-rod. (C) Scattering spectra of the transverse mode (red) with a peak at 520 nm and longitudinal mode (black) mode with a peak at 530 nm and a shoulder at 593 nm, of the quasi-rod.

After the Au-Cu quasi-rods were formed, the alloying process continued to proceed and the NPs grew into regular rod shape. As mentioned above, only one scattering peak was found in single Au nanorods[40, 41], whereas in our experimental study of single Au-Cu alloy nanorods, multiple scattering peaks were observed. In the calculations, we firstly examined the effect of the change in the Au/Cu ratio and in the distribution of Au and Cu atoms in the NPs during growth. Specifically, since the composition of the nanorods changes gradually during the reaction, we varied the fraction of Au and Cu in a nanorod using their respective dielectric constants for their occupied volumes. From the calculations, we observed a change in the scattering peak position when varying the NP composition, but not the split peak pattern. We also compared the spectra when the Au and Cu are well mixed (alloyed) or separated for a given composition and found only slight difference in the spectra (see Supporting Information, Figure S4). This is because that Au and Cu have similar dielectric functions above 550 nm where the resonance wavelengths are located [39, 42]. In the calculations, neither the composition nor the atom distribution in the NPs leads to multiple peaks in the scattering spectra, observed experimentally. Secondly, we considered the effect of glass substrate since the split peak was predicted when a spherical particle was located on a substrate with index of refraction greater than 2[43]. The index of refraction of the glass substrate used in the experiment is about 1.5. When the substrate is included in the calculations, it only red shifts the resonance peak without changing the spectral pattern. Therefore, the substrate effect was treated with effective medium theory[44, 45] in the following simulations. We also examined the change in the size of the NPs and aspect ratios, none of them would produce scattering peaks as shown in the experiments.

We notice that in the alloy NP synthesis, it is hard to form defect-free crystals because the two metals in their pure state have different properties such as atom size, reduction potential, lattice constant and surface energies. These defects may consist of only a few atoms, not easily be detected in normal TEM studies. Since the single particle optical technique is extremely sensitive to the NP geometry, atomic level defects in the Au-Cu nanorods could cause unusual scattering patterns.

To examine the effect of geometric defects in the nanorods on their optical spectra, we calculated the scattering spectra of a 20 nm long Au-Cu alloy nanorod without and with different degrees of defect. To account for the unpolarized excitation light used in the experiments, the scattering spectra presented in Figures 4 and 5 are averaged over different polarizations. For a defect free nanorod as shown in Figure 4A, only a single scattering peak from longitudinal mode of the rod was observed in the calculated spectrum (as shown in Figure 4B). When one well-like defect or two well-shaped defects next to each other were introduced to the rods, peak splitting was observed in the scattering spectra. (HRTEM images are available in Figure S5 in Supporting Information). For an Au-Cu alloy

nanorod with one 0.5 nm wide well like defect (as shown in Figure 4C), its scattering spectrum is extremely sensitive to the well depth. A change of the well depth from 0.75 to 1.0 nm, which corresponds to only one layer of atoms, leads to a split in single longitudinal dipole peak into a dipole peak and an octopole peak (as seen in Figure 4D and supporting information Figure S6 and S7). The defect separates the nanorod into two parts (to its left and right), and the plasmonic coupling between them promotes the generation of octopole peak in such a short rod. For a nanorod with two well-shaped defects arranged close to each other (as shown in Figure 4E), the number of the scattering peaks of the nanorod becomes three. The peak at the longest wavelength corresponds to the dipole mode while the one at the shortest wavelength corresponds to the octopole peak. The peak in between the two is a mixture of the dipole and octopole modes and can hardly be classified clearly. We also attempted structures with defects separated from each other, with similar well defects but different depths, and also structures with asymmetric defects. Multiple peak patterns in the scattering spectra were obtained in each case and splitting was more obvious (see Figure S8, S9 in Supporting Information). The evidence provided by HRTEM and DDA modeling suggests that small structural defects in the nanorods could induce peak splitting. A correlated structural and optical study[46-48] of single Au-Cu nanorod will be pursued in the future to further enhance the study.

As the reaction proceeds, the number of defects decreases due to the formation of nanorods with higher crystallinity. In the optical study, more NPs with a single or two scattering peaks were observed in the NPs acquired at longer reaction times (type IV), in agreement with the theoretical studies. A control experiment when the nanorods were annealed at 280 ºC after 20 minutes reaction show that 50% of the nanorods possess a single scattering peak, compared to 20% before annealing (representative spectra in Supporting Information Figure S10). A quantitative analysis on the number of particles showing multiple and single peaks for different samples shows the number of scattering peaks of the nanorods decreases with reaction time (as shown in Supporting Information Table S1). This proves the geometric defects are indeed the origin of the multiple peak patterns.

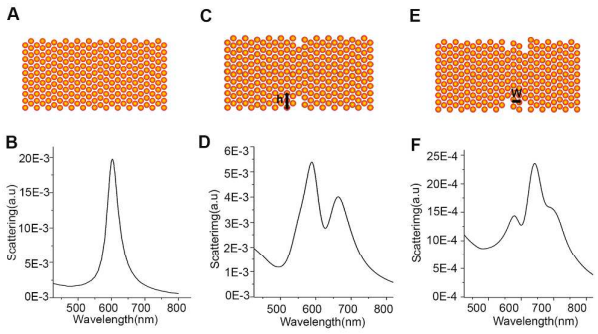

Figure 4. Schemes (A, C and E) and calculated scattering spectra (B, D, and F) of an Au-Cu alloy rod without and with defects. (A-B) Scheme and corresponding scattering spectrum of a rod without defect. (C-D) Scheme and corresponding scattering spectrum of a rod with one well-like defect where the width of the defect is 0.5 nm and the height (h) is 1.25 nm. (E-F) Scheme and corresponding scattering spectrum of a rod with two well-like defects where the defects are 1.5 nm and 1.0 nm in height, and 0.5 nm in width. The defects are separated by a distance (w) of 1.0 nm.

With the understanding of the multiple scattering peaks, we investigate the origin of the red shift in the main scattering peak with increasing reaction time, which was observed in both the single particle and ensemble measurements. In the modeling, we varied the length of the Au-Cu alloy nanorod while keeping a well-like defect of 0.5 nm in width and 1.25 nm in depth (see Figure 5A). The calculated spectra (in Figure 5B) show that the dipole peak of the longitudinal mode red shifts with increasing aspect ratio of the rod, which is expected and consistent with the experimental measurements[49, 50]. The peak intensity of the dipole mode relative to that of the octopole keeps growing which is also in agreement with the measured single particle scattering spectra.

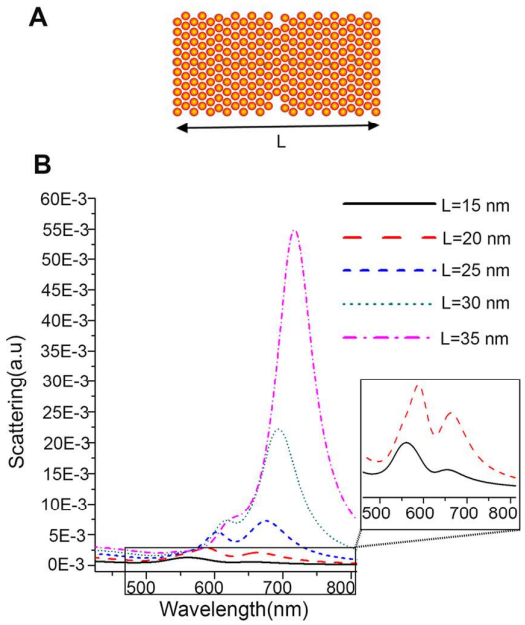

Figure 5. (A) Schematic illustration of a rod with a well-like defect and (B) scattering spectra for the rods of varying lengths. Black: L = 15 nm, Red: L = 20 nm, Blue: L = 25 nm, Sea Green: L = 30 nm, Pink: L = 35 nm.

Possible Mechanisms of Defect Formation

The exact mechanism of defect formation is unknown. We propose here two possible reasons. One is due to the alloy process. Bimetallic alloy NP formation involves diffusing and mixing of two metals. In the alloy process, the crystal structures of the bimetallic NP also change. Since the two metals in their pure state have different properties such as atom size, reduction potential, lattice constant, surface energies, it is challenging for them to form perfect crystals. In our study, as discussed previously, the Cu atoms were deposited on one side of the Au seed before Au and Cu diffused into stable alloy phase. In the diffusing process, the vacancy sites at bimetallic interface before alloying evolve to the surface causing defects mostly on the surfaces of the NPs[24]. As the reaction proceeds, the alloy phase becomes stable $AuCu_3$ and the Au-Cu nanorods also get annealed. Therefore, fewer defects were found in the nanorods at later growth stages.

Another possible reason is that there were unreacted gold precursors ($HAuCl_4$) in the solution while Au-Cu alloy NPs were

forming. Because the reduction potential of $AuCl_4^-$/Au (0.99 V vs SHE) is more positive than of $CuCl_2$/Cu (-0.394 V vs SHE), Cu-rich nanorods can serve as a reduction materials for reaction, being oxidized by $HAuCl_4$ according to

$$3Cu(s) + 2HAuCl_4(aq) \rightarrow 3CuCl_2(s) + 2HCl + 2Au(s)$$

Therefore, the unreacted Au precursor can replace Cu atom from the nanorod surface[51, 52], causing structural defects to form in the nanorods. But the concentration of the Au precursor is not high enough to etch or remove large number of Cu atoms from the centre of the rod, which would result in hollow rod structures. In the experimental condition, we believe only the Cu atoms on the surface of the rods could be replaced by Au atoms, possibly the reason why the kinks are formed on the surface. With increasing reaction time, the concentration of unreacted Au precursors was reduced thus less likely to further remove Cu atoms from the nanorod.

CONCLUSIONS

In summary, single particle scattering spectroscopy was applied to study the growth of single Au-Cu alloy nanorod during synthesis. The single particle scattering spectra have multiple scattering peaks induced by small structural defects and asymmetry in the nanorod geometry. We demonstrated that the single particle scattering spectroscopy can reveal structural defects caused by only a few atoms with the aid of DDA simulations, showing the extreme sensitivity of the optical technique to the NP structure. This method can be applied to study microscopic structural changes at single particle level in alloy systems during synthesis, which significantly affects the properties of the alloy NPs, such as their optical and surface catalytic properties.

Acknowledgements

JZ thanks the UCONN Startup Fund and the American Chemical Society Petroleum Research Fund (PRF# 54004-DN15). SZ thanks the National Science Foundation (NSF ECCS-1238738) and the Office of Naval Research (ONR N00014-0-1-1118) for the support of the research. STEM work made use of shared experimental facilities supported in part by the MRSEC Program of National Science Foundation under award number DMR-1419807.

Notes and references

1. M. B. Cortie and A. M. McDonagh, *Chem. Rev*, 2011, **111**, 3713-3735.
2. M. K. Debe, *Nature*, 2012, **486**, 43-51.
3. B. Lim, M. Jiang, P. H. C. Camargo, E. C. Cho, J. Tao, X. Lu, Y. Zhu and Y. Xia, *Science*, 2009, **324**, 1302-1305.
4. M. G. Blaber, M. D. Arnold and M. J. Ford, *J. Phys: Condens. Mat*, 2010, **22**, 143201.
5. A. L. Schmucker, N. Harris, M. J. Banholzer, M. G. Blaber, K. D. Osberg, G. C. Schatz and C. A. Mirkin, *ACS Nano*, 2010, **4**, 5453-5463.
6. T. Krenke, E. Duman, M. Acet, E. F. Wassermann, X. Moya, L. Manosa and A. Planes, *Nat. Mater.*, 2005, **4**, 450-454.
7. D. M. Alonso, S. G. Wettstein and J. A. Dumesic, *Chem. Soc. Rev.*, 2012, 41, 8075-8098.
8. D. Kim, J. Resasco, Y. Yu, A. M. Asiri and P. Yang, *Nat. Commun.*, 2014, **5**. doi: 10.1038/ncomms5948.
9. N. Wang, Y. Han, Y. Xu, C. Gao and X. Cao, *Anal. Chem.*, 2014, **87**, 457-463.
10. S. Guo, S. Zhang, X. Sun and S. Sun, *J. Am. Chem. Soc.*, 2011, 133, 15354-15357.
11. R. He, Y.-C. Wang, X. Wang, Z. Wang, G. Liu, W. Zhou, L. Wen, Q. Li, X. Wang, X. Chen, J. Zeng and J. G. Hou, *Nat. Commun.*, 2014, **5**. doi: 10.1038/ncomms5327.
12. T. K. Sau and A. L. Rogach, *Adv. Mater.*, 2010, **22**, 1781-1804.
13. A. Walther and A. H. Muller, *Chem. Rev.*, 2013, **113**, 5194-5261.
14. D. Wang and Y. Li, *Adv. Mater.*, 2011, **23**, 1044-1060.
15. J. A. Rodriguez and D. W. Goodman, *Science*, 1992, **257**, 897-903.
16. J. Wu, P. Li, Y.-T. Pan, S. Warren, X. Yin and H. Yang, *Chem. Soc. Rev.*, 2012, **41**, 8066-8074.
17. M. Grzelczak, B. Rodríguez-González, J. Pérez-Juste and L. M. Liz-Marzán, *Adv. Mater.*, 2007, **19**, 2262-2266.
18. F. Tao, M. E. Grass, Y. Zhang, D. R. Butcher, J. R. Renzas, Z. Liu, J. Y. Chung, B. S. Mun, M. Salmeron and G. A. Somorjai, *Science*, 2008, **322**, 932-934.
19. Y. Yang, W. Wang, X. Li, W. Chen, N. Fan, C. Zou, X. Chen, X. Xu, L. Zhang and S. Huang, *Chem. Mater.*, 2012, **25**, 34-41.
20. Z. Quan, Y. Wang and J. Fang, *Acc. Chem. Res.*, 2012, **46**, 191-202.
21. W. J. Huang, R. Sun, J. Tao, L. D. Menard, R. G. Nuzzo and J. M. Zuo, *Nat. Mater.*, 2008, **7**, 308-313.
22. Y. Ding, F. Fan, Z. Tian and Z. L. Wang, *J. Am. Chem. Soc.*, 2010, **132**, 12480-12486.
23. A. I. Frenkel, V. S. Machavariani, A. Rubshtein, Y. Rosenberg, A. Voronel and E. A. Stern, *Phys. Rev. B*, 2000, **62**, 9364-9371.
24. T. Shibata, B. A. Bunker, Z. Zhang, D. Meisel, C. F. Vardeman and J. D. Gezelter, *J. Am. Chem. Soc.*, 2002, **124**, 11989-11996.
25. L. Shi, C. Jing, W. Ma, D.-W. Li, J. E. Halls, F. Marken and Y.-T. Long, *Angew. Chem. Intl. Ed.*, 2013, **52**, 6011-6014.
26. P. Chen, X. Zhou, N. M. Andoy, K.-S. Han, E. Choudhary, N. Zou, G. Chen and H. Shen, *Chem. Soc. Rev.*, 2014, **43**, 1107-1117.
27. B. T. Sneed, C. N. Brodsky, C.-H. Kuo, L. K. Lamontagne, Y. Jiang, Y. Wang, F. Tao, W. Huang and C.-K. Tsung, *J. Am. Chem. Soc.*, 2013, **135**, 14691-14700.
28. H. L. Xin, S. Alayoglu, R. Tao, A. Genc, C.-M. Wang, L. Kovarik, E. A. Stach, L.-W. Wang, M. Salmeron, G. A. Somorjai and H. Zheng, *Nano Lett.*, 2014, **14**, 3203-3207.
29. B. T. Sneed, C.-H. Kuo, C. N. Brodsky and C.-K. Tsung, *J. Am. Chem. Soc*, 2012, **134**, 18417-18426.
30. N. J. Halas, S. Lal, W.-S. Chang, S. Link and P. Nordlander, *Chem. Rev.*, 2011, **111**, 3913-3961.
31. V. Giannini, A. I. Fernández-Domínguez, S. C. Heck and S. A. Maier, *Chem. Rev.*, 2011, **111**, 3888-3912.
32. M. A. van Dijk, M. Lippitz and M. Orrit, *Acc. Chem. Res.*, 2005, **38**, 594-601.
33. C. Novo, A. M. Funston and P. Mulvaney, *Nat. Nano.*, 2008, **3**, 598-602.
34. J. G. Smith, Q. Yang and P. K. Jain, *Angew. Chem. Intl. Ed.*, 2014, **53**, 2867-2872.
35. P.-C. Chen, G. Liu, Y. Zhou, K. A. Brown, N. Chernyak, J. L. Hedrick, S. He, Z. Xie, Q.-Y. Lin, V. P. Dravid, S. A. O'Neill-

Slawecki and C. A. Mirkin, *JACS.*, 2015, DOI: 10.1021/jacs.5b05139.
36. G. Liu, D. J. Eichelsdoerfer, B. Rasin, Y. Zhou, K. A. Brown, X. Liao and C. A. Mirkin, *PNAS.*, 2013, **110**, 887-891.
37. S. Chen, S. V. Jenkins, J. Tao, Y. Zhu and J. Chen, *J. Phys. Chem. C*, 2013, **117**, 8924-8932.
38. T. B. Draine, *The Astrophys. J.*, 1988, **333**, 848-872.
39. E. D. Palik, *Handbook of optical constants of solids*, Academic Press, Boston, 1988.
40. H. Chen, L. Shao, Q. Li and J. Wang, *Chem. Soc. Rev.*, 2013, **42**, 2679-2724.
41. L. S. Slaughter, Y. Wu, B. A. Willingham, P. Nordlander and S. Link, *ACS Nano*, 2010, **4**, 4657-4666.
42. A. Bansal and S. S. Verma, *AIP Advances*, 2014, **4**, 057104.
43. J. Lermé, C. Bonnet, M. Broyer, E. Cottancin, D. Manchon and M. Pellarin, *J. Phys. Chem. C*, 2013, **117**, 6383-6398.
44. X. Tian, Y. Zhou, S. Thota, S. Zou and J. Zhao, *J Phys. Chem. C*, 2014, **118**, 13801-13808.
45. M. Wang and N. Pan, *Mater. Sci. Eng. R.*, 2008, **63**, 1-30.
46. E. M. Perassi, C. Hrelescu, A. Wisnet, M. Döblinger, C. Scheu, F. Jäckel, E. A. Coronado and J. Feldmann, *ACS Nano*, 2014, **8**, 4395-4402.
47. A. Grubisic, V. Schweikhard, T. A. Baker and D. J. Nesbitt, *ACS Nano*, 2013, **7**, 87-99.
48. Q. Wei, H. Qi, W. Luo, D. Tseng, S. J. Ki, Z. Wan, Z. Göröcs, L. A. Bentolila, T.-T. Wu, R. Sun and A. Ozcan, *ACS Nano*, 2013, **7**, 9147-9155.
49. S. Link and M. A. El-Sayed, *J. Phys. Chem. B*, 1999, **103**, 8410-8426.
50. L. Vigderman and E. R. Zubarev, *Chem. Mater.*, 2013, **25**, 1450-1457.
51. Y. Sun and Y. Xia, *Science* 2002, **298**, 2176-2179.
52. C. W. Yen, M. A. Mahmoud and M. A. El-Sayed, *J. Phys. Chem. A* 2009, **113**, 4340-4345.

TOC :

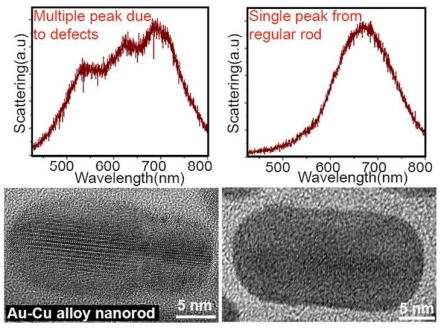

Structural defects induce splitting in the plasmon bands of Au-Cu alloy nanorod during growth compared to a defect free alloy nanorod.